Plasmon canalization and tunneling over anisotropic metasurfaces

Diego Correas-Serrano, Andrea Alù, and J. Sebastian Gomez-Diaz

Phys. Rev. B **96**, 075436 — Published 28 August 2017

DOI: 10.1103/PhysRevB.96.075436

Plasmon Canalization and Tunneling over Anisotropic Metasurfaces

Diego Correas-Serrano[1], Andrea Alù[2□], and J. Sebastian Gomez-Diaz[1*]

[1]Department of Electrical and Computer Engineering, University of California, Davis
One Shields Avenue, Kemper Hall 2039, Davis, California 95616, USA
[2]Department of Electrical and Computer Engineering, The University of Texas at Austin
1616 Guadalupe Street, UTA 7.215, Austin, Texas 78701, USA
□ alu@mail.utexas.edu *jsgomez@ucdavis.edu

We discuss the possibility of plasmon canalization, collimation, and tunneling over ultrathin metasurfaces, enabled by extreme anisotropy in their complex conductivity dyadic. The interplay between anisotropy, conductivity-near-zero, and loss is exploited here to derive general conditions for plasmon canalization and efficient energy transport. We also demonstrate how the intrinsic in-plane anisotropy of black phosphorus can provide a natural platform to engineer these conditions, exhibiting important advantages over isotropic plasmonic materials. Our findings have implications for plasmonic sensors, planar hyperlenses and plasmon steering over a surface, and they highlight the potential of 2D materials beyond graphene.

PACS: 42.25.Bs, 73.20.Mf., 78.67.Pt.

I. INTRODUCTION

Anisotropic metamaterials have enabled the control of light in ways unreachable with conventional materials, giving rise to exotic electromagnetic phenomena such as negative refraction, hyperbolic dispersion, manipulation of the evanescent spectrum, drastic emission enhancement, cloaking, and electromagnetic transparency, to name a few [1]–[5]. Recently, extreme anisotropy in the conductivity – i.e., Im[$\bar{\bar{\varepsilon}}$]– of ε-near-zero (ENZ) metamaterials has been shown to enable the counterintuitive

phenomenon of energy collimation and omnidirectional enhancement of transmission between dissimilar media, even for grazing incidence [6], [7]. These findings have triggered the pursuit of practical implementations of this phenomenon not only at radiofrequencies and optical frequencies but also in acoustics [8], [9]. Current electromagnetic realizations rely on 3D metamaterials, that not only suffer from well-known issues like challenging fabrication and large volumetric loss [1], [10], [11], but also present no advantage over thin films in terms of near-field interactions with external sources [12]. Consequently, most designs have focused on the collimation of propagating waves impinging from free space into the ENZ medium, limiting the maximum spatial resolution transmitted therein to the light cone. Implementations of this concept over ultrathin plasmonic metasurfaces (MTSs), on the contrary, would enable more ambitious applications with increased resolution and simpler excitation, processing, and retrieval of light via near-field techniques [13].

Simple raw translations of bulk ENZ concepts into 2D MTSs [13]–[16] have led to promising σ-near-zero configurations that exhibit light canalization [11], [13] by engineering the imaginary part of the conductivity dyad, but relegate the real part of the conductivity to a mere hindrance [17]. This strategy not only misses the potential of loss-enhanced canalization available in bulk materials [6], [10], but also fails to incorporate the actual response of plasmonic materials into the design, leading to complex implementations with suboptimal performances [17].

In this paper, we derive general conditions for collimation and canalization of SPPs over extremely anisotropic MTSs, and we propose optimal designs based on the unusual anisotropic optical properties of black phosphorus [18]–[23], which enables better performance than isotropic plasmonic materials like graphene or noble metals. For this purpose, we start by investigating the dispersion relation, field distributions, and energy transport of surface plasmon polaritons (SPPs) as a function of loss anisotropy. We show quite counterintuitively that specific forms of loss anisotropy can facilitate energy transport over a surface, rather than harming it. Then, we exploit this property to unveil two-dimensional loss-induced canalization and collimation of highly confined and directional SPPs in ultrathin MTSs over

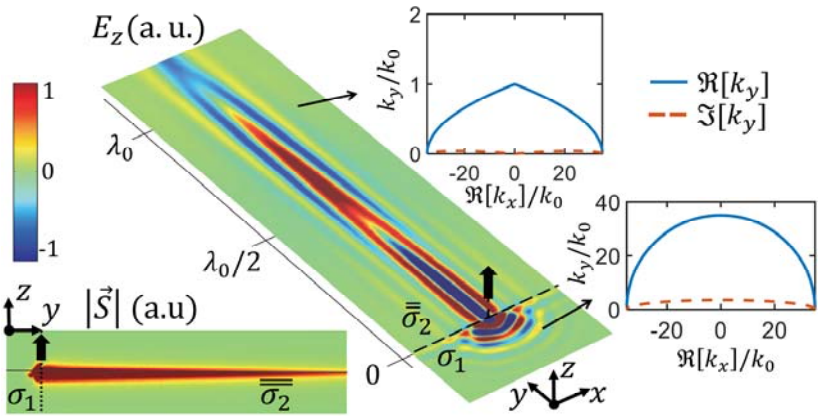

Fig. 1. Excitation of surface waves by a z-oriented dipole (black arrow) located 15 nm above the interface between two inductive (metallic-like) metasurfaces placed in free-space. The first metasurface is isotropic with conductivity $\sigma_1 = 0.015 + i0.15$ mS, thus supporting isotropic TM plasmons (see bottom right inset). The second metasurface is defined by a diagonal conductivity tensor $\bar{\bar{\sigma}}_2 = \left(\sigma_2^{xx}, 0; 0, \sigma_2^{yy}\right)$, where $\sigma_1 = \sigma_2^{xx}$, $\mathrm{Im}[\sigma_2^{yy}] = \mathrm{Im}[\sigma_2^{yy}]$, and $\mathrm{Re}[\sigma_2^{yy}] \to \infty$, and supports low-loss quasi-TEM plasmons in the canalization regime (see top right inset). Color plots show the electric field E_z and the absolute value of the Poynting vector $\vec{S}$ over the structure surface (central) and transverse plane (left bottom), respectively.

longer distances than isotropic plasmons. Although this scenario has some connections with loss-induced canalization in the bulk [6], the reduced dimensionality of MTSs imposes additional constraints and provides new knobs to engineer the supported plasmons, enabling much richer near-field interactions, collimation of the evanescent spectrum, and the corresponding enhancement of the spontaneous emission rate from nearby sources [13].

The general concept of loss-based canalization is illustrated in Fig. 1. A z-oriented dipole is placed above an interface between two inductive metasurfaces with complex conductivities σ_1 and $\bar{\bar{\sigma}}_2$. The conductivity σ_1 is plasmonic and isotropic, supporting confined transverse-magnetic (TM) SPPs that decay due to absorption, whereas the tensor conductivity $\bar{\bar{\sigma}}_2$ is highly loss-anisotropic with $\mathrm{Re}[\sigma_{yy}] \to \infty$ (equal to σ_1 for the other tensor elements). The plasmon isofrequency contours (IFCs) in the insets show that the maximum wavenumber allowed along the x-direction (k_x) is the same in both cases, since $\sigma_{xx}^1 = \sigma_{xx}^2$, but the corresponding values of k_y are very different. The extreme anisotropy in $\bar{\bar{\sigma}}_2$ causes the real and imaginary parts of the IFC to flatten, resulting in collimated plasmons that are highly confined to the surface, travel longer distances along specific directions than in the isotropic case, and retain the same

transverse resolution in *x*. This loss-induced canalization regime is a particular case of the general canalization schemes described in this paper.

II. THEORY OF PLASMON CANALIZATION AND TUNNELING

The dispersion relation, field distribution and energy transport properties of surface plasmons supported by free-space standing anisotropic metasurfaces defined by $\bar{\bar{\sigma}} = \sigma_{xx}\hat{x}\hat{x} + \sigma_{yy}\hat{y}\hat{y}$ can be derived by finding the states of a system described by the equation [24]

$$\left(E_x\hat{x} + E_y\hat{y}\right) \cdot \left(\bar{\bar{Z}}\bar{\bar{\sigma}} + 2\bar{\bar{I}}\right) = 0 \#(1)$$

where

$$\bar{\bar{Z}} = \frac{\omega\mu_0}{k_z}\left(I - \frac{1}{k_0^2}\bar{k}_t \cdot \bar{k}_t\right) \#(2)$$

$\bar{\bar{I}}$ is the unitary dyad, k_0 is the free-space wavenumber, $\bar{k}_t = k_x\hat{x} + k_y\hat{y}$ and $k_z = \sqrt{k_0^2 - k_x^2 - k_y^2}$. The wavevector of the propagating states corresponds to the eigenvalues of the matrix $\left(\bar{\bar{Z}}\bar{\bar{\sigma}} + 2\bar{\bar{I}}\right)$, which yields the dispersion relation**Error! Reference source not found. Error! Reference source not found.**

$$2k_0^2\eta(\sigma_{xx} + \sigma_{yy}) - 2\eta\left(k_x{}^2\sigma_{xx} + k_y^2\sigma_{yy}\right) + k_0k_z\left(4 + \eta^2\sigma_{xx}\sigma_{yy}\right) = 0. \#(3)$$

This equation describes all possible bound modes over homogeneous metasurfaces, whose characteristics depend on the values of σ_{xx} and σ_{yy}. This includes isotropic TM (metallic-like, $\mathrm{Im}[\sigma\,] > 0$), TE (dielectric-like, $\mathrm{Im}[\sigma\,] < 0$), propagation, anisotropic elliptical hybrid TM/TE modes ($\sigma_{xx} \neq \sigma_{yy}$), hyperbolic plasmons $\mathrm{sgn}(\mathrm{Im}[\sigma_{xx}]) \neq \mathrm{sgn}\left(\mathrm{Im}\left[\sigma_{yy}\right]\right)$, and the canalization regime on which we focus [11], [13]. From Refs. [13], [17], SPP propagation is strongly favored along *y* when $\left|\mathrm{Im}\left[\sigma_{yy}\right]\right| \gg |\mathrm{Im}[\sigma_{xx}]|$, a scenario that usually appears when $|\mathrm{Im}[\sigma_{xx}]| \approx 0$, i.e. the so called σ-near-zero response. This behavior was first observed in bulk metamaterials, where canalization has usually been obtained in ENZ structures [4], [10], [25]. Recently, loss-induced canalization has been demonstrated in bulk metamaterials when $\mathrm{Im}[\varepsilon_\perp] \gg \mathrm{Im}[\varepsilon_\parallel]$, see Refs. [6], [8], [10]. We note that the term "loss-induced*"* used to describe this phenomenon may lead to confusion, as increasing the imaginary part of ε does not

necessarily imply an increase in loss [26]. A simple example is the case of a perfect conductor, for which the imaginary part of permittivity tends to infinity, but its large value prevents the field from entering the metal and therefore avoids absorption. Anyhow, these studies have demonstrated the possibility of realizing exotic responses by tailoring the material conductivity, which is typically treated as a nuisance in metamaterials. Analyzing the response of anisotropic MTSs we realize that ideal canalization along *y* can be achieved either when $\mathrm{Im}[\sigma_{yy}] \to \pm\infty$ or when $\mathrm{Re}[\sigma_{yy}] \to \infty$. The former case is the so-called *σ-near-zero response* [11], [13] whereas we refer to the latter as *loss-induced plasmon canalization* [5]–[7]. Importantly, both cases lead to a consistent response and field distribution that holds independently of the topology (elliptic or hyperbolic) of the metasurface. The dispersion relation simplifies to

$$k_y = k_0\sqrt{1+\frac{k_z\eta\sigma_{xx}}{2k_0}}, \#(4)$$

where η and k_0 are the free-space impedance and wavenumber, respectively, and $k_0^2 = k_x^2 + k_y^2 + k_z^2$ holds.

In the non-retarded regime, Eq. (4) can be further simplified by noting that $k_z \approx \pm ik_x$, implying that ideal canalization occurs if $|\sigma_{xx}| \to 0$, leading to $k_y = k_0$ for all k_x. In practice, realistic implementations will force a closing of the IFC through a finite value of σ_{xx} or spatial dispersion effects [19], [27]–[29]. Neglecting the latter, canalization remains near perfect for $|\mathrm{Re}[k_x]| \ll 2k_0/(\eta|\mathrm{Im}[\sigma_{xx}]|)$, where the sign of σ_{xx} (plasmonic, $\mathrm{Im}[\sigma_{xx}] > 0$, or dielectric, $\mathrm{Im}[\sigma_{yy} < 0]$) have a small effect on phase and energy propagation, as well as on the polarization of the fields, as will be shown below. However, and somewhat counterintuitively, σ_{xx} should not always be made as small as possible, as σ_{xx} not only affects the maximum k_x supported by the metasurface, but also modifies the entire IFC and the associated propagation loss. This can be deduced from Eq. (4) by fixing k_x (assuming $k_z \approx \pm ik_x$) and decreasing σ_{xx}, which implies larger complex k_y, and faster decay in *y*.

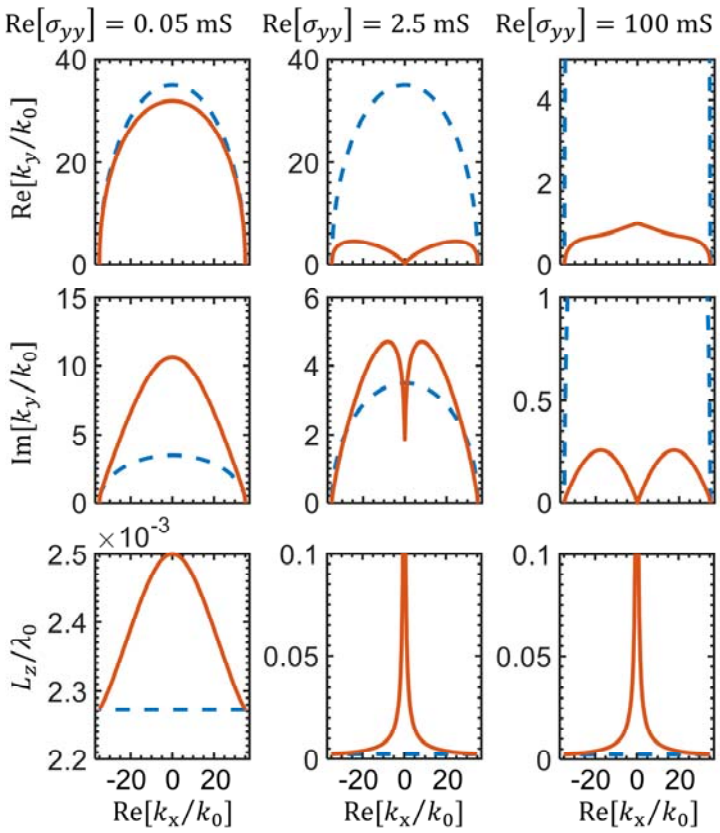

Fig. 2. Influence of $\mathrm{Re}[\sigma_{yy}]$ on the isofrequency contour and transverse confinement of SPPs supported by uniaxial metasurfaces with anisotropic elliptical response. The structures are defined by $\bar{\bar{\sigma}} = (\sigma_{xx}, 0; 0, \sigma_{yy})$, where $\sigma_{yy} = \mathrm{Re}[\sigma_{yy}] + i0.15$ mS and $\sigma_{xx} = 0.015 + i0.15$ mS. The right column illustrates loss-based plasmon canalization. Results are computed (solid line) for $\mathrm{Re}[\sigma_{yy}] = 0.05, 2.5$ and 100 mS. Results for a baseline isotropic MTS with conductivity $\sigma = 0.015 + i0.15$ mS are included for reference (blue dashed line). L_z is the distance of 1/e power decay away from the MTS.

The simplified scenario described by Eq. (4) assumes that $\mathrm{Re}[\sigma_{yy}]$ or $\mathrm{Im}[\sigma_{yy}]$ are infinitely large, but the picture is different for finite conductivity profiles. In this case, moderate values of $\mathrm{Im}[\sigma_{yy}]$ can enhance plasmon propagation and directionality, whereas $\mathrm{Re}[\sigma_{yy}]$ remains detrimental unless larger values can be achieved. Fig. 2 illustrates this scenario by showing the IFC and transverse confinement of plasmons in increasingly loss-anisotropic MTSs (orange, solid lines), with $\sigma_{xx} = 0.015 + i0.15$ mS and $\sigma_{yy} = \mathrm{Re}[\sigma_{yy}] + i0.15$ mS. In all panels, blue dashed lines correspond to the baseline isotropic metasurface with $\sigma_{yy} = \sigma_{xx} = 0.015 + i0.15$ mS. Note that these calculations do not correspond yet to any physical implementation, but are used to clearly illustrate the physics of this class of metasurfaces. The left

column, with $\mathrm{Re}[\sigma_{yy}] = 0.05$ mS, illustrates how slightly increasing the unidirectional loss has a detrimental effect on plasmon propagation, with higher attenuation for all supported k_x, in agreement with the conventional wisdom that $\mathrm{Re}[\sigma_{yy}]$ should be as small as possible in plasmonic MTSs. The added loss has a small effect on the transverse confinement L_z, defined as the distance from the metasurface with 1/*e* power decay. Further increasing the conductivity to 2.5 mS (middle column) leads to a qualitatively different topology, as the high uniaxial loss leads to strong plasmon decay in the *y* direction ($\mathrm{Im}[k_y] > \mathrm{Re}[k_y]$) with all spatial frequencies predominantly traveling towards $\pm x$, as will be detailed below concerning energy transport. Confinement to the surface is now significantly reduced for low-k_x due to their quasi-plane wave nature, but moderate-to-high k_x, which carry subwavelength information and are of highest practical interest in plasmonics due to their miniaturization capabilities, increased field enhancement, and resolution for lensing applications, remain sufficiently confined [11]. Finally, the right column shows the desired canalization response, with $\mathrm{Re}[\sigma_{yy}] = 100$ mS. The IFC is now almost flat for $|\mathrm{Re}[k_x]| < 2k_0/(\eta|\mathrm{Im}[\sigma_{xx}]|)$ and decay is slow, implying canalization of a wide range of spatial frequencies, while the transverse confinement remains almost identical to the previous scenario despite the completely different in-plane characteristics. This behavior is explained by the uniaxial loss being sufficiently large to forbid electric fields in the *y* direction for *all* surface waves, preventing SPP-like wavelength shrinkage *in this direction* (hence the small k_y) and dramatically lowering absorption. We stress that this response is completely general and appears in any metasurface by significantly increasing $\mathrm{Im}[\sigma_{yy}]$ or $\mathrm{Re}[\sigma_{yy}]$, independently of its topology. Results for moderate values of $\mathrm{Im}[\sigma_{yy}]$ can be readily computed with our theoretical framework, leading to topologies reported in previous works [11], [13], [17].

A complete description of plasmon propagation over this class of metasurfaces requires studying the polarization direction of energy transport, which in anisotropic media differs from the direction of phase propagation and is given by the Poynting vector $\vec{S} = \frac{1}{2}\mathrm{Re}[\vec{E} \times \vec{H}]$. The in-plane components of the

electric field, E_x and E_y are found as the eigenvectors of the matrix $\left(\bar{\bar{Z}}\bar{\bar{\sigma}} + 2\bar{\bar{I}}\right)$, with the transverse component E_z and the magnetic field $\vec{H}$ readily retrieved from Maxwell's equations. For arbitrary σ_{xx} and σ_{yy} they take the form

$$E_x = Ae^{i\vec{k}\cdot\vec{r}},$$

$$E_y = Ae^{i\vec{k}\vec{r}}\frac{2\,k_x k_y \sigma_{xx}}{-\sigma_{xx}(k_0^2 - k_x^2) + \sigma_{yy}\left(k_0^2 - k_y^2\right) \pm C},$$

$$E_z = Ae^{i\vec{k}\cdot\vec{r}}\frac{1}{2\,k_x k_z \sigma_{yy}}\left(-(k_0^2 - k_x^2)\sigma_{xx} + (k_z^2 - k_x^2)\sigma_{yy} \mp C\right), \#$$

$$H_x = -Ae^{i\vec{k}\vec{r}}\frac{k_x k_y}{\omega\mu_0\, k_z}\frac{(k_0^2 - k_x^2)\sigma_{xx} + \left(k_0^2 - k_y^2\right)\sigma_{yy} \pm C}{-(k_0^2 - k_x^2)\sigma_{xx} + \left(k_0^2 - k_y^2\right)\sigma_{yy} \pm C}, \qquad \#(5)$$

$$H_y = Ae^{i\vec{k}\cdot\vec{r}}\frac{1}{2\,k_z\mu_0\omega\,\sigma_{yy}}\left(\sigma_{xx}(k_0^2 - k_x^2) + \sigma_{yy}\left(k_0^2 - k_y^2\right) \pm C\right), \#$$

$$H_z = Ae^{i\vec{k}\cdot\vec{r}}\frac{1}{2\,k_y\mu_0\omega\sigma_{yy}}\left(\sigma_{xx}(k_0^2 - k_x^2) - \sigma_{yy}\left(k_0^2 + k_y^2\right) \pm C\right), \#$$

where A is an arbitrary field amplitude, and

$$C = \pm\sqrt{k_0^4\left(\sigma_{xx} - \sigma_{yy}\right)^2 - 2\,k_0^2\left(\sigma_{xx} - \sigma_{yy}\right)\left(k_x^2\sigma_{xx} - k_y^2\sigma_{yy}\right) + \left(k_x^2\sigma_{xx} + k_y^2\sigma_{yy}\right)^2}. \#(6)$$

The signs of the square roots must be chosen to make the eigenvectors correspond to the proper eigenvalues ($\vec{k}$ depicted in the IFCs). We remark that these expressions are valid for all types of metasurface plasmon topologies, including isotropic, elliptical, and hyperbolic plasmons [11] and, to the best of our knowledge, they are not available elsewhere. They can be applied beyond the scope of this paper to engineer effective coupling and matching mechanisms for hyperbolic and extremely anisotropic plasmons, and to exploit their unusual properties to design devices based on engineering the characteristic impedance and wavevector, like switches, phase shifters, or filters [30].

If $\left|\sigma_{yy}\right| \to \infty$, the above expressions can be greatly simplified, providing valuable insight into the polarization of the canalized plasmons. In this case, C can be written as

$$\mathrm{C} = \pm\sigma_{yy}\left(k_y^2 - k_0^2\right), \#(7)$$

leading to

$$E_x = Ae^{i\vec{k}\cdot\vec{r}}; E_y = 0; E_z = -A\frac{k_x}{k_z}e^{i\vec{k}\cdot\vec{r}}$$

$$H_x = \frac{A\,k_y k_x}{\omega\mu_0 k_z}e^{i\vec{k}\cdot\vec{r}}; H_y = -\frac{A}{\omega\mu_0}\frac{k_z^2 + k_x^2}{k_z}e^{i\vec{k}\cdot\vec{r}}; H_z = \frac{A}{\omega\mu_0}k_y e^{i\vec{k}\cdot\vec{r}} \#(8)$$

All surface plasmons in canalization are TE with respect to *y*, which is expected given that $|\sigma_{yy}| \to \infty$. By closely inspecting Eq. (8), one realizes that in the usual non-retarded regime (where $k_z \approx \pm ik_x$ when $|\sigma_{xx}| \to 0$) $H_y \to 0$, hence all the supported surface plasmons are quasi-TEM and circularly polarized with respect to the propagation direction.

The Poynting vector $\vec{S} = \frac{1}{2}\mathrm{Re}\left[\vec{E} \times \vec{H}^*\right]$ can now be calculated rigorously. In the canalization regime, it simplifies to

$$S_x = A^2 \cdot \Re\left[\frac{k_x}{k_z}\left(\frac{k_x^2+k_z^2}{k_z}\right)^* e^{2\vec{k}\vec{r}}\right],\ S_y = A^2 \cdot \Re\left[k_y^*\left(1 + \left|\frac{k_x}{k_z}\right|^2\right)e^{2\vec{k}\vec{r}}\right],\ S_z = A^2 \cdot \Re\left[\left(\frac{k_x^2+k_z^2}{k_z}\right)^* e^{2\vec{k}\vec{r}}\right], \quad (9)$$

Note that k_z is imaginary for lossless σ_{xx}, and therefore $S_z = 0$. Otherwise, $|S_z| > 0$ represents the power flow towards the metasurface from fields above and below, where it is dissipated. In the non-retarded regime, Eq. (9) simplifies to $S_x = 0$, $S_y = 2A\mathrm{Re}\left[k_y\right]$, and $S_z = 0$, implying that, ideally, all propagating energy is collimated towards *y*.

Fig. 3 shows the electric and magnetic field components for the anisotropic MTSs studied in Fig. 2, as well as the direction of the Poynting vector $\angle\vec{S} = \tan^{-1}\left(\frac{S_x}{S_y}\right)$ computed using the exact expressions detailed above. Results are plotted versus k_x (the corresponding k_y can be retrieved from Fig. 2). The left column corresponds to the near-isotropic case, with quasi-TM propagation ($H_z = 0$ in isotropic TM plasmons) and $\angle\vec{S}$ very similar to the baseline isotropic metasurface (blue dashed lines in bottom row). In the middle column, corresponding to the overdamped case studied in Fig. 2, plasmon polarization is remarkably different, with stronger E_x, $H_z \approx H_x$, and energy propagation predominantly towards $\pm x$.

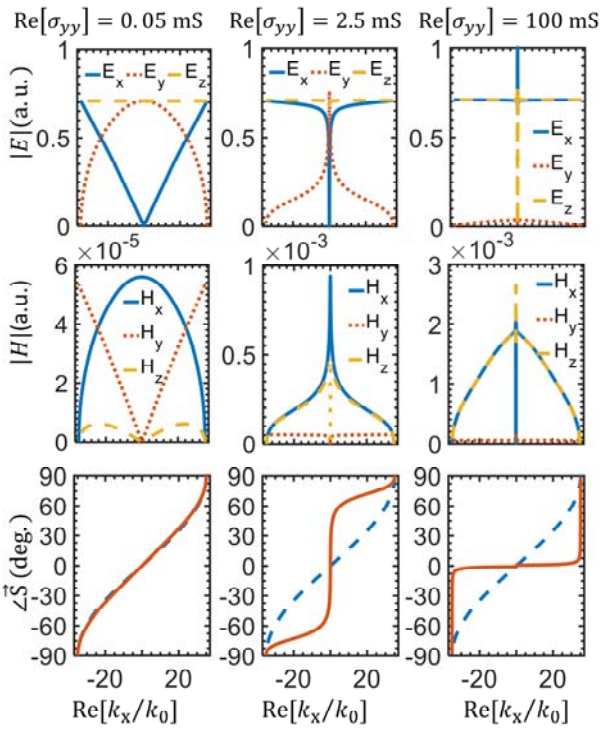

Fig. 3. Polarization (top and middle row) and direction of the Poynting vector (bottom row) of the SPPs supported by the metasurfaces described in Fig. 2 versus k_x for $z = 0$. Fields are normalized such that $|\vec{E}| = 1$ on the metasurface (at $z = 0$). Direction of the Poynting vector $\angle\vec{S}$ (deg) is measured from the *y*-direction. The blue dashed lines in bottom row correspond to the baseline isotropic metasurface in Fig. 2.

Finally, the right column showcases the canalization scenario, demonstrating the quasi-TEM nature deduced from Eq. (8) and almost perfect canalization ($\angle S = 0$) for all supported surface waves except those with $k_y = 0$. Interestingly, close to this operation point, energy can be directed from 0 to 90 degrees with very small variations of k_x. This extreme response has not been observed before and we envision it could be exploited to efficiently steer plasmons over a surface by using reconfigurable materials like graphene or black phosphorus to shift this operation through σ_{xx}.

In idealized 3D metamaterials, it has been shown that when *propagating* waves impinge from free-space onto the loss-enhanced medium at an oblique angle ($k_x > 0$, with $\hat{x}$ parallel to the interface), the transmitted beam propagates towards y. In the 2D scenario under study, the supported k_x spectrum is mostly *evanescent* - falling outside the light cone - and can be easily excited and retrieved by through near-field techniques. Loss-enhanced MTSs couple and then collimate the impinging waves, *but also*

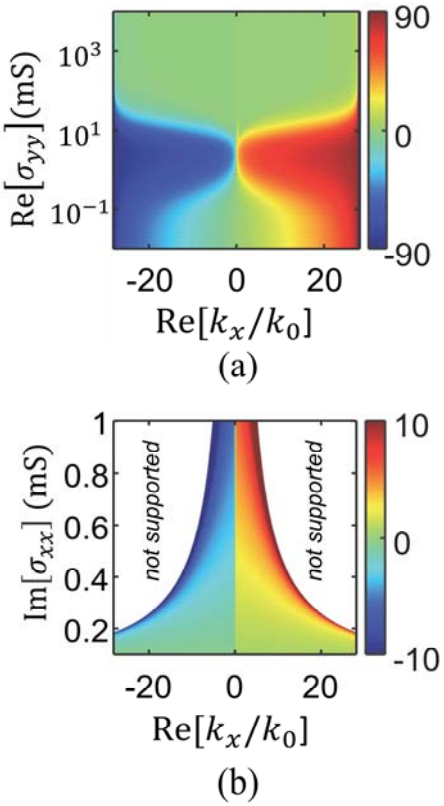

Fig. 4. Collimation properties of surface plasmons over uniaxial metasurfaces. (a)-(b) In-plane direction of power propagation ($\angle\vec{S}$ in degrees) of the supported SPPs versus their x wavenumbers. Results are shown as a function of (a) $\mathrm{Re}[\sigma_{yy}]$, with $\sigma_{yy} = \mathrm{Re}[\sigma_{yy}] + i0.15$ mS and $\sigma_{xx} = 0.015 + i0.15$ mS, and (b) versus $\mathrm{Im}[\sigma_{xx}]$, with $\sigma_{yy} = \infty + i0.15$mS and $\sigma_{xx} = 0.015 + i\mathrm{Im}[\sigma_{xx}]$ mS.

significantly increase the spontaneous emission rate of the emitter itself [13]. In the particular case of Fig. 2, if the k_x component of incoming evanescent waves or surface plasmons falls within the supported range (roughly between -35k_0 and +35k_0), the coupled energy will propagate towards y in the form of confined surface waves, as predicted by Eq. (4). Fig. 4 completes the study of energy transport over anisotropic metasurfaces. Panel (a) allows to clearly identify the three distinct regimes previously described. With low loss, the metasurface is nearly isotropic and energy transport depends strongly on k_x ($\angle\vec{S} \approx \angle\vec{k}$). As loss increases, it first triggers the most detrimental regime (overdamped plasmons towards $\pm x$) before finally enabling the desired loss-based canalization response. The right panel highlights the importance of the σ-near zero condition along x for a fixed $\mathrm{Re}[\sigma_{yy}] = 100$ mS, as increasing $\mathrm{Im}[\sigma_{xx}]$ leads not only to a reduced maximum spatial resolution, but also to more energy spread for any given k_x,

illustrating the interplay between σ_{yy} and σ_{xx} in the response to the entire angular spectrum and the necessity of deliberate metasurface designs.

III. IMPLEMENTATION USING BLACK PHOSPHORUS METASURFACES

To engineer this class of metasurfaces, we explore the use of intrinsically anisotropic 2D materials and exploit the natural contrast between their conductivity components. This approach opens unprecedented venues to manipulate the in-plane optical conductivity of the resulting structures, and allows to easily implement elliptical and hyperbolic plasmon topologies [13] with additional design flexibility associated to the in-plane material anisotropy. Here, we apply this platform to achieve SPP canalization and collimation. Previous implementations have always been based on suboptimal σ-near zero topologies realized by modulating graphene conductivity [17] or simply by arranging graphene or silver strips [13], [14]. These structures employed isotropic materials to engineer MTSs with $\mathrm{Im}[\sigma_{yy}] \approx 0$, leaving loss and the transverse conductivity component as an important hindrance. Instead of isotropic materials, we exploit here the strong in-plane optical anisotropy of black phosphorus (BP) [19], which is ideal to fulfill the stringent and conflicting conditions required for SPP canalization. BP is a 2D material with high electron mobility, moderate bandgap and its in-plane properties can be tuned both electrically and mechanically [18], [20], [23], [31], [32], placing it somewhere in between graphene and transition metal dichalcogenides [33]. Recently, it has been shown that BP supports strongly confined anisotropic surface plasmons at mid-IR (an elusive band for graphene and metal plasmonics [34]), exhibiting unprecedented rich topologies and looser field confinement bounds than graphene [19].

Fig. 5 shows a near-optimal metasurface able to implement loss-based plasmon canalization and collimation through an array of subwavelength BP ribbons. Optimal performance requires strips oriented along the zig-zag direction (with high-inductance σ_{ZZ} conductivity), while the armchair direction (with low inductance σ_{AC} conductivity) creates a lossy resonance in combination with the capacitive near-field coupling between strips. Fig. 5b shows the real and imaginary parts of σ_{AC} and σ_{ZZ} for a 3 nm thin film

with chemical potential of 0.38 eV and a scattering rate of 2 meV that phenomenologically accounts for all loss mechanisms, including scattering from impurities and phonons, Landau damping, etc. [35], [36]. The metasurface is designed to exhibit a high loss resonance in the mid-IR (implementing the $\mathrm{Re}[\sigma_{yy}] \rightarrow \infty$ condition), requiring a period of $L = 40\,\mathrm{nm}$ and ribbon width $W = 37\,\mathrm{nm}$. The local effective conductivity along *x* and *y*, extracted from numerical simulations [38], is shown in 5c. The design has been conducted using a simple but powerful effective medium approach detailed in [11], [24], which predicts the resonant frequency and conductivity tensor of this metasurface with an error of less than 1%. This approach is based on modelling the strip near-field coupling as an effective capacitance [37]

$$C_{eff} = (2L\varepsilon_0/\pi)\log\left(\frac{1}{\sin\left(\frac{\pi(L-W)}{2L}\right)}\right). \#(10)$$

The conductivity along *x* and *y* may then be expressed as

$$\sigma_{xx}^{eff} = \frac{W}{L}\sigma_{ZZ} \quad \text{and} \quad \sigma_{yy}^{eff} = \left(\frac{1}{\sigma_{AC}} + \frac{i}{\omega C_{eff}}\right)^{-1}, \#(11)$$

where *W* and *L* are the strip width and the unit cell period. The resonant frequency is designed to be around 78.5 THz, with $\sigma_{yy}^{eff} = 143\,\mathrm{mS}$ and $\sigma_{xx}^{eff} = 0.5 + 57i\,\mu\mathrm{S}$ (with an anisotropic ratio of $|\sigma_{yy}|/|\sigma_{xx}| \approx 2500$). In the effective medium limit, the IFC and $\angle\vec{S}$ of the plasmons supported by this metasurface are shown in Fig. 5d. This metasurface presents exceptional canalization capabilities, with a nearly flat IFC for $k_x < 100k_0$ and moderate loss [39]. If an isotropic material like graphene was used instead, any pre-determined $\mathrm{Re}[\sigma_{yy}^{eff}]$ in the design would be associated with a larger σ_{xx}^{eff} due to the isotropic in-plane conductivity, reducing the range of supported k_x (see Fig. 4b). Conversely, fixing σ_{xx}^{eff} would lead to lower σ_{yy}^{eff}. Black phosphorus, however, is the ideal platform to simultaneously create a suitable resonance and extend the range of supported k_x. This implementation is not possible using noble metals either, whose low inductance at THz and infrared cannot induce the required resonance nor support large spatial frequencies. Our proposed metasurface can be fabricated using standard e-beam lithography and, although inherently narrowband, its operation frequency can be tuned in real time by

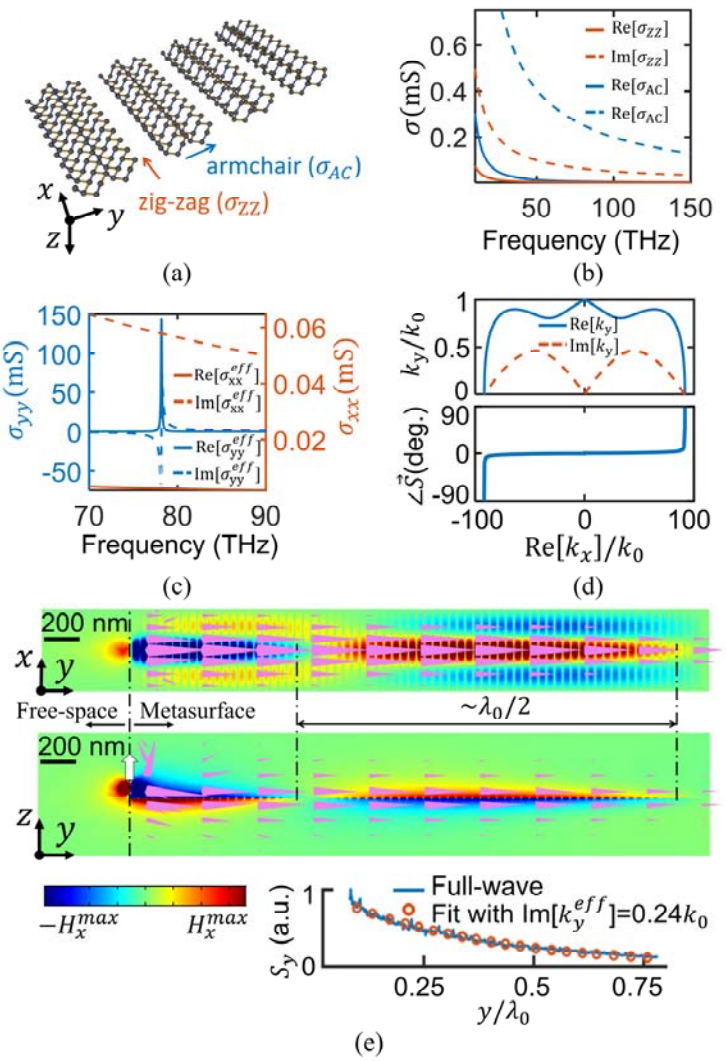

Fig. 5. Loss-induced collimation of quasi-TEM plasmons over an array of black phosphorus nanoribbons (a) Metasurface with ribbons oriented along the zig-zag direction, the high inductance axis. (b) Kubo conductivity of a 3-nm black phosphorus film with chemical potential $\mu_c = 0.38$ eV along the armchair and zig-zag directions. (c) Effective MTS in-plane conductivity along the *x* and *y* directions. (d) Isofrequency contour of the quasi-TEM waves along this MTS. (e) *x*-component of the magnetic field (H_x, colormap) and Poynting vector (arrows, in logarithmic scale) induced by a *z*-oriented dipole (white arrow in bottom panel) 60 nm above the proposed MTS. Inset shows the power decay along *y* (dashed black line) and a fit to a single exponential decay profile $S_y \propto e^{-2\mathrm{Im}[k_y^{eff}]y}$, with $k_y^{eff} = 0.24k_0$.

electrical doping or mechanical modulations [38]–[40]. We remark that all strips can be biased simultaneously by a single contact or tuned by an elastic substrate, enabling straightforward topological transitions [13], on-off switching of canalization and collimation for specific frequencies, narrowband tunable filters, or for temporary isolation of sensitive detectors.

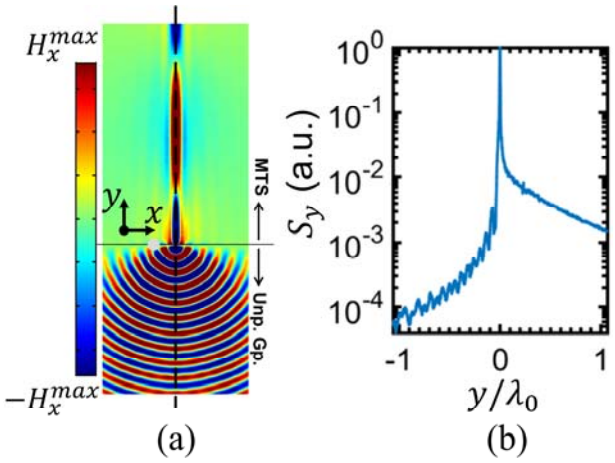

Fig. 6. Power decay along the metasurface from Fig. 4 (y>0, MTS) and along unpatterned graphene (y<0, Unp. Graphene) when excited by the same z-oriented dipole. (a) x-component of the magnetic field, H_x. (b) y-component of the Poynting vector along the dashed line of panel, λ_0 being the free-space wavelength.

To validate the canalization capabilities of the proposed structure, we simulated its response to a *z*-oriented electric dipole located 60 nm above it. Results have been computed using COMSOL Multiphysics [40]. Fig. 5e shows the *x*-component of the magnetic field and the Poynting vector (arrows, size in logarithmic scale). The collimation properties of the MTS are clear, with a narrow plasmon beam confined to the surface and propagating entirely towards *y*, i.e. $k_y \approx k_0$. The direction and magnitude of the Poynting vector confirm that power propagates in a highly-directed beam, since all spatial frequencies excited by the dipole propagate with $\angle\vec{S} = 0$. Fig. 5e also shows the total power decay rate along dashed line (z=50 nm), which can be approximated as $\mathrm{S_y} \propto \mathrm{e}^{-2\mathrm{Im}\left[\mathrm{k_y^{eff}}\right]\mathrm{y}}$ with effective $\mathrm{k_y^{eff}} = \mathrm{i}0.24\mathrm{k_0}$. As expected, this "effective" value $\mathrm{Im}\left[\mathrm{k_y^{eff}}\right]$, which depends on the excitation, is within the range of the values shown in the IFC, between 0 to 0.5 approximately.

To further highlight how directional energy transport is enhanced by the proposed metasurface, we compare it to the case of unpatterned graphene. The same dipole source is now placed above the interface between the proposed metasurface, now characterized by its effective medium conductivity tensor, and an infinite graphene sheet with the same scattering rate and chemical potential as the constituent black phosphorus strips ($\eta = 2$ meV, $\mu_c = 0.38$ eV). Fig. 6 shows the *x*-component of the magnetic field in the metasurface plane, with the bottom panel showing the *y*-component of the Poynting vector along the

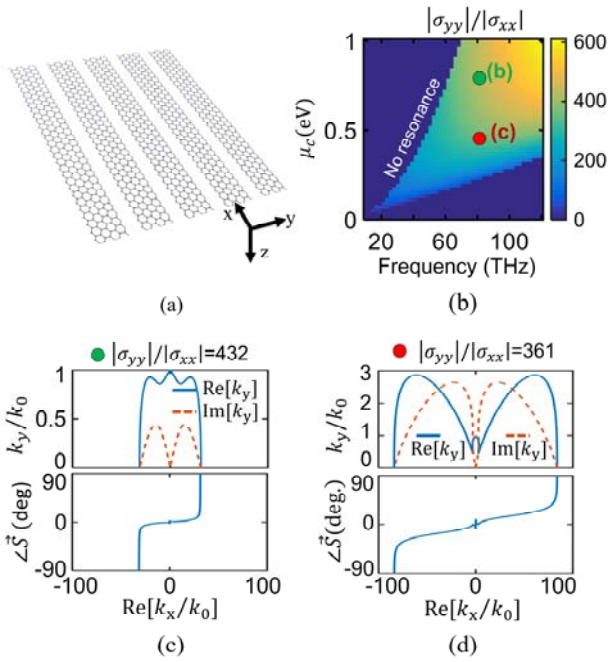

Fig. 7. Canalization using free-standing resonant graphene strip MTSs (scattering rate $\eta = 2$ meV). The green dot corresponds to a design that can satisfactorily implement canalization with similar decay rate as the BP MTS of Fig. 5a, although limited to a narrower range of k_x. The red dot design supports a similar range of k_x as the BP MTS, but canalization performance is poor.

dashed line. In graphene, energy spreads in all directions whereas the black phosphorus metasurface forces it to remain in a narrow beam, resulting in a slower decay rate along y and more efficient energy transport, as depicted in Fig. 6b.

Lastly, we stress that to successfully implement plasmon canalization in this type of metasurfaces, it is not enough to arbitrarily design a plasmonic strip array resonating at the desired frequency. This type of resonance has been reported in several papers on graphene metasurfaces [11], [13], [27], [41] as the analogue of resonances found in layered uniaxial metamaterials, but it has never been shown to enable this unusual canalization regime since it must be adequately designed to this end. Here we show that, taking this into account, graphene can also be used to implement loss-based canalization, although the isotropic nature of graphene is not as suitable for designing extremely anisotropic metasurfaces. Consider the metasurface depicted in Fig. 7a, comprised of graphene strips modeled through the Kubo formula with a scattering rate of $\eta = 2$ meV [42], [43] to take interband transitions into account. For simplicity, photon-phonon coupling and associated losses in graphene are not considered. This is a somewhat

arbitrary comparison, as any real device will require additional practical considerations like substrate compatibility, but it allows to further illustrate the potential of BP in the familiar context of graphene plasmonics. Fig. 7b shows the degree of anisotropy at the resonance of the structure versus frequency and chemical potential. We aim to design a metasurface with performance comparable to the BP one at the same frequency of 78 THz, using the same unit cell period of 40 nm. The green dot marks a design point ($\mu_c = 0.83$ eV) that successfully implements canalization with similar damping along y. However, compared to the BP implementation, the range of canalized k_x is less than half, (the IFC closes around $k_x \approx 33k_0$). The red dot, on the other hand, corresponds to a metasurface designed to exhibit similar transverse resolution (IFC closing around $k_x = 100k_0$), achieved with $\mu_c = 0.48$ eV. In this case, however, plasmon damping is high and canalization imperfect, with large $\mathrm{Im}[k_y]$. Note, in both cases, that the anisotropy ratio $|\sigma_{yy}|/|\sigma_{xx}|$ is much lower than in the BP metasurface: 432 and 361 versus 2500. These results illustrate the advantage of using of intrinsically anisotropic materials like black phosphorus in designing extremely anisotropic metasurfaces.

IV. CONCLUSIONS

In this paper, we have provided a rigorous framework for plasmon canalization and collimation over anisotropic metasurfaces, focusing on loss-enhanced responses. An analysis in terms of dispersion, polarization, and energy transport has revealed that this is a particular case of general conditions for plasmon canalization over metasurfaces, which have been studied in detail. The proposed implementation based on black phosphorus strips exploits the intrinsic in-plane anisotropy of this material to enhance the response of plasmonic metasurfaces and demonstrates important advantages over isotropic 2D materials like graphene, hinting at enormous potential for future applications. The structure is designed using an effective medium approach and analyzed with full-wave simulations, showing strong capabilities to canalize infrared light in a dynamically reconfigurable fashion. We envision that astute use of anisotropic

conductivity and absorption in metasurfaces may open new exciting directions in metasurface technology for in-plane plasmon steering, lensing, and sensing.

Acknowledgement

A.A. acknowledges support of the Air Force Office of Scientific Research with grant No. FA9550-17-1-0002, the National Science Foundation, the Welch Foundation with grant No. F-1802, and the Simons Foundation.

APPENDIX: CANALIZATION IN A HYPERBOLIC METASURFACE

In the main text, all results shown correspond to metasurfaces with inductive σ_{xx}, i.e. $\mathrm{Im}[\sigma_{xx}] > 0$. Plasmon canalization is also supported for hyperbolic metasurfaces, i.e. $\mathrm{Im}[\sigma_{xx}] < 0$ [11], [13], [14] as long as the conditions $|\sigma_{yy}| \to \infty$ and $|\sigma_{xx}| \to 0$ are met. Fig. 8 shows the real and imaginary parts of the isofrequency contour as well as the direction of energy propagation of surface plasmons in hyperbolic metasurfaces with increasingly anisotropic loss, in a similar fashion as Fig. 2 and 3. The same regimes are identified, transitioning from regular hyperbolic topologies (blue dashed lines) to overdamped plasmons (left column), to canalization (middle and right column), but a key difference is observed: the value of $\mathrm{Re}[k_y]$ also determines the range of supported k_x, whereas it was solely determined by σ_{xx} in elliptic MTSs. In the overdamped regime, the metasurface does not support surface waves, whereas in canalization, the spatial resolution can be enhanced by increasing $\mathrm{Re}[\sigma_{yy}]$, as demonstrated in Fig. 8. We also note that the hyperbolic metasurface considered here required $\mathrm{Re}[\sigma_{yy}] = 300$ mS to achieve similar performance as the the elliptic metasurface from Fig. 2, with $\mathrm{Re}[\sigma_{yy}] = 100$ mS.

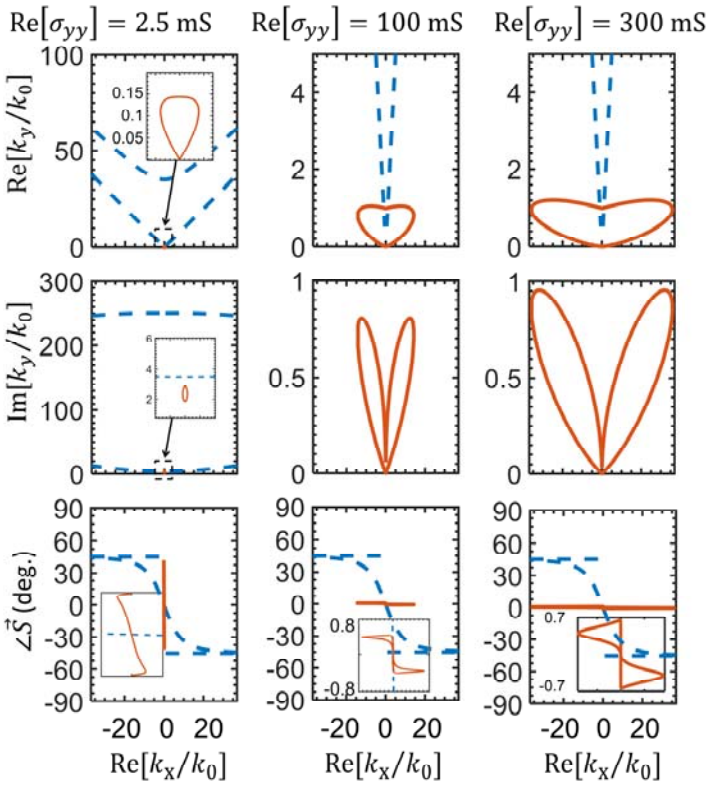

Fig. 8. Canalization of surface plasmons in hyperbolic metasurfaces with anisotropic loss. The structures are defined by $\bar{\bar{\sigma}} = (\sigma_{xx}, 0; 0, \sigma_{yy})$, where $\sigma_{yy} = \text{Re}[\sigma_{yy}] + i0.15$ mS and $\sigma_{xx} = 0.015 - i0.15$ mS. Results for a baseline hyperbolic MTS with conductivity $\sigma_{yy} = 0.015 + i0.15$ mS are included for reference (blue dashed line).

REFERENCES

[1] A. Poddubny, I. Iorsh, P. Belov, and Y. Kivshar, "Hyperbolic metamaterials," *Nat. Photonics*, vol. 7, no. 12, pp. 948–957, Nov. 2013.

[2] Y. Guo and Z. Jacob, "Thermal hyperbolic metamaterials.," *Opt. Express*, vol. 21, no. 12, pp. 15014–9, 2013.

[3] I. S. Nefedov, A. J. Viitanen, and S. A. Tretyakov, "Propagating and evanescent modes in two-

dimensional wire media," *Phys. Rev. E - Stat. Nonlinear, Soft Matter Phys.*, vol. 71, no. 4, pp. 1–10, 2005.

[4] M. Silveirinha and N. Engheta, "Tunneling of electromagnetic energy through subwavelength channels and bends using epsilon-near-zero materials," *Phys. Rev. Lett.*, vol. 97, no. 15, p. 157403, 2006.

[5] J. Gomis-Bresco, D. Artigas, and L. Torner, "Anisotropy-Induced Photonic Bound States in the Continuum," *Nat. Photonics*, p. accepted, 2017.

[6] S. Feng, "Loss-Induced Omnidirectional Bending to the Normal in □ -near-Zero Metamaterials," *Phys. Rev. Lett.*, vol. 108, no. 9, pp. 0–2, 2012.

[7] L. Sun, S. Feng, and X. Yang, "Loss enhanced transmission and collimation in anisotropic epsilon-near-zero metamaterials," *Appl. Phys. Lett.*, vol. 101, no. 24, 2012.

[8] K. Yu, Z. Guo, H. Jiang, and H. Chen, "Loss-induced topological transition of dispersion in metamaterials," *J. Appl. Phys.*, vol. 119, no. 20, pp. 1–6, 2016.

[9] C. Shen and Y. Jing, "Loss-induced enhanced transmission in anisotropic density-near-zero acoustic metamaterials," *Sci. Rep.*, pp. 1–13, 2016.

[10] N. H. Shen, P. Zhang, T. Koschny, and C. M. Soukoulis, "Metamaterial-based lossy anisotropic epsilon-near-zero medium for energy collimation," *Phys. Rev. B - Condens. Matter Mater. Phys.*, vol. 93, no. 24, p. 245118, 2016.

[11] J. S. Gomez-Diaz and A. Alu, "Flatland Optics with Hyperbolic Metasurfaces," *ACS Photonics*, vol. 3, no. 12, p. acsphotonics.6b00645, 2016.

[12] O. D. Miller, S. G. Johnson, and A. W. Rodriguez, "Effectiveness of thin films in lieu of hyperbolic metamaterials in the near field," *Phys. Rev. Lett.*, vol. 112, no. 15, pp. 1–5, 2014.

[13] J. S. Gomez-Diaz, M. Tymchenko, A. Alù, and A. Alu, "Hyperbolic Plasmons and Topological Transitions over Uniaxial Metasurfaces," *Phys. Rev. Lett.*, vol. 114, no. 23, p. 233901, 2015.

[14] A. a. High *et al.*, "Visible-frequency hyperbolic metasurface," *Nature*, vol. 522, no. 7555, pp.

192–196, 2015.

[15] M. Khorasaninejad, W. T. Chen, R. C. Devlin, J. Oh, A. Y. Zhu, and F. Capasso, “Metalenses at visible wavelengths: Diffraction-limited focusing and subwavelength resolution imaging,” *Science (80-.).*, vol. 352, no. 6290, pp. 1190–1194, 2016.

[16] N. Mohammadi Estakhri and A. Alù, “Wave-front Transformation with Gradient Metasurfaces,” *Phys. Rev. X*, vol. 6, no. 4, p. 41008, 2016.

[17] E. Forati, G. W. Hanson, A. B. Yakovlev, and A. Alù, “Planar hyperlens based on a modulated graphene monolayer,” *Phys. Rev. B - Condens. Matter Mater. Phys.*, vol. 89, no. 8, pp. 1–5, 2014.

[18] F. Xia, H. Wang, and Y. Jia, “Rediscovering black phosphorus as an anisotropic layered material for optoelectronics and electronics.,” *Nat. Commun.*, vol. 5, p. 4458, Jul. 2014.

[19] D. Correas-Serrano, J. S. Gomez-Diaz, A. A. Melcon, and A. Alù, “Black phosphorus plasmonics: anisotropic elliptical propagation and nonlocality-induced canalization,” *J. Opt.*, vol. 18, no. 10, p. 104006, 2016.

[20] T. Low *et al.*, “Tunable optical properties of multilayers black phosphorus,” *Phys. Rev. B - Condens. Matter Mater. Phys.*, vol. 75434, no. 7, pp. 1–5, Apr. 2014.

[21] X. Wang and S. Lan, “Optical properties of black phosphorus,” *Adv. Opt. Photonics*, vol. 8, no. 4, p. 618, 2016.

[22] T. Low *et al.*, “Polaritons in layered two-dimensional materials,” *Nat. Mater.*, 2016.

[23] K. Khaliji, A. Fallahi, L. Martin-Moreno, and T. Low, “Tunable plasmon-enhanced birefringence in ribbon array of anisotropic 2D materials,” no. 4, pp. 4–8, 2017.

[24] D. L. Sounas and C. Caloz, “Gyrotropy and nonreciprocity of graphene for microwave applications,” *IEEE Trans. Microw. Theory Tech.*, vol. 60, no. 4, pp. 901–914, Apr. 2012.

[25] V. Y. Fedorov and T. Nakajima, “All-angle collimation of incident light in μ-near-zero metamaterials,” *Opt. Express*, vol. 21, no. 23, p. 27789, 2013.

[26] J. D. Jackson, *Classical Electrodynamics, section 8.1*. Wiley Online Library, 1975.

[27] D. Correas-Serrano, J. S. Gomez-Diaz, M. Tymchenko, and A. Alù, "Nonlocal response of hyperbolic metasurfaces," *Opt. Express*, vol. 23, no. 23, p. 29434, 2015.

[28] T. Christensen, W. Yan, S. Raza, A. P. Jauho, N. A. Mortensen, and M. Wubs, "Nonlocal response of metallic nanospheres probed by light, electrons, and atoms," *ACS Nano*, vol. 8, no. 2, pp. 1745–1758, 2014.

[29] C. David, J. Christensen, N. A. Mortensen, and I. G. Mill, "Spatial dispersion in two-dimensional plasmonic crystals: Large blueshifts promoted by diffraction anomalies," *Phys. Rev. B - Condens. Matter Mater. Phys.*, vol. 94, no. 16, p. 165410, 2016.

[30] D. Correas-Serrano, J. S. Gomez-Diaz, J. Perruisseau-Carrier, and A. Alvarez-Melcon, "Graphene-based plasmonic tunable low-pass filters in the terahertz band," *IEEE Trans. Nanotechnol.*, vol. 13, no. 6, pp. 1145–1153, Nov. 2014.

[31] J. Lu *et al.*, "Bandgap Engineering of Phosphorene by Laser Oxidation toward Functional 2D Materials," *ACS Nano*, vol. 9, no. 10, pp. 10411–10421, Oct. 2015.

[32] J. Kim *et al.*, "Observation of tunable band gap and anisotropic Dirac semimetal state in black phosphorus," *Science (80-.).*, vol. 349, no. 6249, pp. 723–726, 2015.

[33] R. Mas-Ballesté *et al.*, "2D materials: to graphene and beyond.," *Nanoscale*, vol. 3, no. 1, pp. 20–30, Jan. 2011.

[34] M. Jablan, H. Buljan, and M. Soljačić, "Plasmonics in graphene at infrared frequencies," *Phys. Rev. B - Condens. Matter Mater. Phys.*, vol. 80, no. 24, p. 245435, Dec. 2009.

[35] S. A. H. Gangaraj, T. Low, A. Nemilentsau, and G. W. Hanson, "Directive Surface Plasmons on Tunable Two-Dimensional Hyperbolic Metasurfaces and Black Phosphorus: Green's Function and Complex Plane Analysis," *IEEE Trans. Antennas Propag.*, vol. 65, no. 3, pp. 1174–1186, Mar. 2017.

[36] T. Low *et al.*, "Plasmons and screening in monolayer and multilayer black phosphorus," *Phys. Rev. Lett.*, vol. 113, no. 10, pp. 3–5, Sep. 2014.

[37] O. Luukkonen *et al.*, "Simple and Accurate Analytical Model of Planar Grids and High-Impedance Surfaces Comprising Metal Strips or Patches," vol. 56, no. 6, pp. 1624–1632, 2008.

[38] A. S. Rodin, A. Carvalho, and A. H. Castro Neto, "Strain-induced gap modification in black phosphorus," *Phys. Rev. Lett.*, vol. 112, no. 17, pp. 1–5, May 2014.

[39] R. Fei and L. Yang, "Strain-engineering the anisotropic electrical conductance of few-layer black phosphorus," *Nano Lett.*, vol. 14, no. 5, pp. 2884–2889, 2014.

[40] S. Yuan, E. Van Veen, M. I. Katsnelson, and R. Roldán, "Quantum Hall effect and semiconductor-to-semimetal transition in biased black phosphorus," *Phys. Rev. B - Condens. Matter Mater. Phys.*, vol. 93, no. 24, pp. 1–6, 2016.

[41] J. S. Gomez-Diaz, M. Tymchenko, and A. Alù, "Hyperbolic metasurfaces: surface plasmons, light-matter interactions, and physical implementation using graphene strips," *Opt. Mater. Express*, vol. 5, no. 10, p. 2313, Oct. 2015.

[42] A. H. Castro Neto, F. Guinea, N. M. R. Peres, K. S. Novoselov, and A. K. Geim, "The electronic properties of graphene," *Rev. Mod. Phys.*, vol. 81, no. 1, pp. 109–162, 2009.

[43] G. W. Hanson, "Dyadic Green's functions for an anisotropic non-local model of biased graphene," *IEEE Trans. Antennas Propag.*, vol. 56, no. 3, pp. 747–757, Mar. 2008.